Factors Affecting the Stability of *T*-Tail Transports

ROBERT T. TAYLOR* AND EDWARD J. RAY*
NASA Langley Research Center, Hampton, Va.

A wind-tunnel research program has been undertaken by NASA to study the aerodynamic characteristics of *T*-tail aircraft at high angles of attack. The program was designed to show the effect on longitudinal stability and control of several configuration variables encompassing horizontal-tail size, vertical position, planform, and incidences; nacelle size, location, and pylon effects; wing section, stall-control devices, flaps, aspect ratio, and sweep; fuselage cross-sectional size, cross-sectional shape, and forebody length. Results of this program are presented and analyzed to serve as a guide to preliminary design.

Nomenclature

b	=	wing span
C_L	=	lift coefficient
$(C_m)_{0.40\bar{c}}$	=	pitching-moment coefficient about $0.40\bar{c}$
ΔC_{m_t}	=	incremental moment due to horizontal tail
$\bar{c}$	=	wing mean aerodynamic chord
i_t	=	tail incidence
Δi_t	=	change in tail incidence
l_t	=	tail arm
M	=	Mach number
S	=	wing reference area
S_t	=	tail area
z	=	tail height
α	=	angle of attack
α_{stall}	=	angle of attack at wing stall
α_t	=	angle of attack of horizontal tail
η	=	angle-of-attack factor, $C_{mi_t}/(C_{mi_t})_{\alpha=0}$
ϵ	=	downwash angle, deg
$(dC_N/d\alpha)_t$	=	"installed" tail normal-force-coefficient slope
i_w	=	wing incidence
λ	=	wing taper ratio
$\bar{V}_t$	=	tail volume coefficient, $(S_t/S)(l_t/\bar{c})$
C_{mi_t}	=	"installed" control effectiveness of horizontal tail, dC_m/di_t

Introduction

THE current trend to design aircraft with high horizontal tails and engines mounted on the aft fuselage has led to concern over the stability characteristics of these aircraft at angles of attack before and beyond the stall. The possibility of inadvertent excursions to extremely high angle of attack has been shown in a number of flight tests where stalling maneuvers were being performed.

The *T*-tail offers advantages in performance because of the lower wetted area of the horizontal- and vertical-tail combination. The horizontal tail is in a region where, from a point of view of stability and control at normal-flight angles of attack, it is very effective because of reduced downwash rate and nearly full dynamic pressure. In addition, the horizontal tail tends to endplate the vertical tail, and thereby increases the effectiveness of this surface.[1]

Research in the past has concentrated on providing acceptable stability characteristics up to the angle of attack at which the wing stalls. Reference 2 summarizes this effort and provides a foundation upon which the selection of wings and appropriate tail locations may be based, which leads to satisfactory stability characteristics in the range prior to wing stall. At the stall and beyond, however, Ref. 2 points to the inevitable fact that the high tail must ultimately penetrate the wake system of the airplane, and once this penetration has taken place, the tail loses effectiveness.

NASA has undertaken a wind-tunnel research program to investigate the post-stall or high-angle-of-attack aerodynamic characteristics of configurations using the *T*-tail. Table 1 shows the scope of the wind-tunnel tests. The program was designed to study the effects on longitudinal stability and control of many configuration variables, primarily at low speed. Reference 3 gave a preliminary review of the experimental program and a summary of the important results to that time.

The experimental program on post-stall stability studies has been continued at Langley Research Center. The purpose of this present paper is to analyze in more detail some of the results of Ref. 3 and to present information acquired since then which may be of use to the preliminary design engineer in obtaining acceptable stability characteristics with the *T*-tail.

Discussion

Basic Configuration

Figure 1 shows a line drawing of one configuration of the model used in the wind-tunnel tests. It is typical of the current *T*-tail aircraft in that it has a wing with moderate sweepback and aft-mounted engine nacelles. Some pertinent model dimensions are given in terms of the wing mean aerodynamic chord $\bar{c}$ and wing span b. Throughout this paper, the aerodynamic characteristics of this configuration will be used as a standard of comparison and will be referred to as the "basic configuration."

Experimental work regarding the pitchup associated with swept-wing aircraft is summarized in Ref. 2. Figure 2 has been taken directly from Ref. 2 and is reproduced here to show the general areas in which these modern aircraft fall in regard to wing geometry and tail location. The boundaries on wing aspect ratio and sweep shown are those required for satis-

Table 1 Scope of the wind-tunnel research program[a]

Item	Variations
Horizontal tail	Size, vertical position, planform, and incidence
Nacelle	Size and location
Wing	Section, stall control devices, flaps, aspect ratio, and sweep
Fuselage	Cross-sectional size, cross-sectional shape, forebody length

[a] Mach number: 0.21 to 0.90; Reynolds number: 0.78×10^6 to 3.0×10^6.

Presented as Preprint 65-737 at the AIAA/RAeS/JSASS Aircraft Design and Technology Meeting, Los Angeles, Calif., November 15–18, 1965; submitted December 18, 1965; revision received April 13, 1966.

* Aerospace Engineer, Stability and Performance Branch, Full-Scale Research Division.

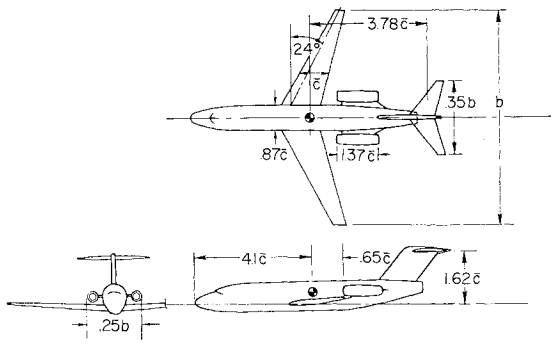

Fig. 1 General arrangement of basic configuration.

factory wing-body stability characteristics at two values of the wing taper ratio, $\lambda = 0$ and 1.0. These curves are applicable to conventional planforms at the low speeds used for these tests.

The current T-tail transport aircraft generally fall in the shaded region on the chart, although there are some exceptions. It should be noted here that the boundaries shown are only approximate, and, depending on the design of the airfoil section and the wing twist selected, the line shown may broaden, but, in general, the hatched band is in a region where fairly well-behaved stability characteristics might be expected for the wing-body. The wings used throughout the present study are shown on the chart as numbered symbols. These wings covered the moderate sweep and aspect ratio range shown. At the Mach number used for most of the tests, the stall pattern on all of the wings was well behaved, as indicated by the wing positions on the chart in relation to the boundaries.

The boundaries for tail location are shown as functions of the nondimensional tail height $z/\bar{c}$ and tail arm $l_t/\bar{c}$. Four areas are shown: A is the region generally associated with T-tails and indicates the pitchup at high lift to be preceded by stall warning. The area of tail position immediately beneath, labeled B, usually yields pitchup without warning regardless of the wing planform chosen. Area C indicates tail locations that are satisfactory for operation below the critical Mach number, and those in area D generally show no pitch-up. It should be noted that the boundaries shown were based on data that did not include the possible effects of engine nacelles, and the range of angle of attack was limited in most cases to a few degrees beyond the primary wing stall. The band of tail location for airplanes with aft nacelles is shown as a hatched area. It should be noted that both sets of boundaries were drawn for wings of conventional planform.

In order to verify the boundaries when the configuration includes engine nacelles aft on the fuselage, the effect of tail height was re-examined, and the range of angle of attack was extended. The circled symbols on the chart designate the several tail heights that were tested with aft fuselage-mounted nacelles.

Effect of Tail Height

The effect of tail height is shown in Fig. 3 as curves of the variation of pitching-moment coefficient with angle of attack for three tail heights. Generally speaking, there is no effect of the nacelle in the low-angle-of-attack range. These curves show the effects predicted by Fig. 2, that is, when the tail is either very low or very high, the curves are well behaved prior to wing stall. The solid curves in each case represent data trimmed at an angle of attack of 10°, and the dashed curve represents an incremental incidence of 4°($\Delta i_t = 4°$) and serves to illustrate the effect of angle of attack on control effectiveness. With the tail mounted in or very near the wing-chord plane, $z/\bar{c} = 0$, both the static stability and the control characteristics appear satisfactory at and beyond the trim point shown. As the tail is moved to a height of $z/\bar{c} = 0.91$, a nonlinearity is evident in the data, starting at about the $\alpha = 10°$ trim point, which is caused by the tail entering the airplane wake system. The wake system in this discussion is taken not only as low-energy air usually associated with the wake, but also as air that has attained large downwash as a result of the wing lift system. The control effectiveness loss is shown by a comparison of the arrows at the first and second trim points. The midtail does not suffer greatly in this respect. A point not to be overlooked here is the tendency to "pitchup" in the lift region prior to wing stall if the tail is located midway up the fin. It should also be noted that the tail while entering the wake system ($\alpha = 10°$) emerges early, and after $\alpha \approx 20°$ the curves are well behaved.

Increasing the tail height to $z/\bar{c} = 1.62$ (data for the basic configuration) illustrates the source of concern with the T-tail. The curves are fairly well behaved up to the point where the wing stalls; at this point, the tail enters the model wake system, and the curves tend to degenerate and exhibit a stable trim point at an angle of attack of 40°. There is also a marked reduction in the control effectiveness at the second trim point which can be seen by comparing the length of the arrows. The control available for recovery from high-angle-of-attack penetrations is a small fraction of its initial low-lift value.

In this paper, it is assumed that control is available to recover from any angle of attack to which the aircraft may be flown or may penetrate. The prime concern here is the region of positive unstable moment on the stability curve shown hatched in Fig. 3, since this type of moment variation creates the problem of inadvertent penetration to higher than the initial trim angle. This type of variation must precede a high-angle stable trim point. Most modern aircraft have very effective high-lift systems and require very powerful stabilizers not only to trim the flap moment but also to allow for loading over a wide range of center-of-

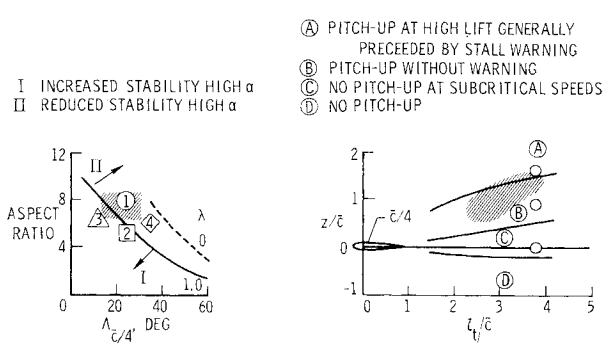

Fig. 2 Stability boundaries for wing geometry and tail location.[1]

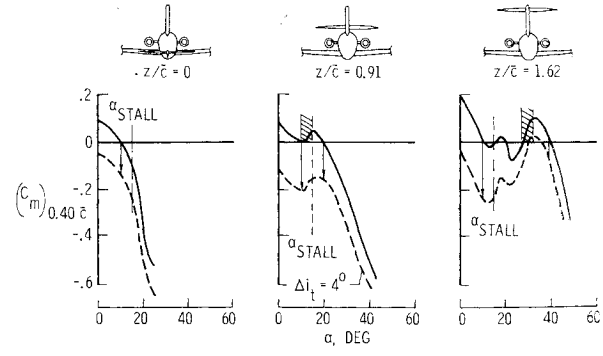

Fig. 3 Effect of horizontal tail height ($M = 0.21$, $\bar{V}_t = 0.83$).

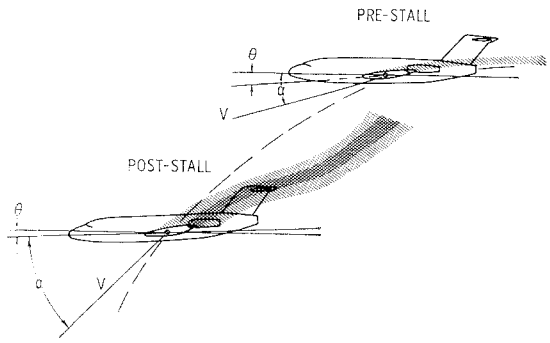

Fig. 4 Wake flow patterns.

gravity locations. The additional control power required is a definite asset in the T-tail aircraft at high angles of attack.

Some feeling for what happens at the very high angles of attack may be obtained from Fig. 4, which shows sketches of the flow in the region of the tail before and after wing stall. In the top of the figure, the region of the low-energy wakes is shown to pass below the location of the T-tail. After the wing stall, however, as the angle of attack develops, the airplane wake system envelopes the tail, and the wing wake is reinforced by the nacelle wake. Simulator studies as well as the instrumented flights mentioned earlier have indicated a tendency for the attitude in the so-called deep stall to be relatively flat with very high negative flight-path angles, as illustrated in Fig. 4. (As a result, the gyro reference is apt to be a misleading cue to angle of attack in all but steady level flight, as pointed out by several investigations, for example, Ref. 4.)

The influence on pitching moment of the complete airplane flowfield in the region of the tail is best assessed by an examination of the pitching-moment equation.

Flowfield Considerations

A review of the equation for the static pitching-moment coefficient is given here:

$$C_m = \underbrace{(\Delta C_m)_{\text{fuselage}} + (\Delta C_m)_{\text{wing}} + (\Delta C_m)_{\text{nacelle}}} + (\Delta C_m)_{\text{tail}}$$

The equation shown has been divided into the contribution of the wing-body nacelle plus the contribution of the tail. The tail contribution can be written as follows:

$$(\Delta C_m)_{\text{tail}} = \left(\frac{dC_N}{d\alpha}\right)(\alpha_t)\left(\frac{S_t}{S}\,\frac{l_t}{\bar{c}}\right)\left(\frac{q_t}{q}\right)$$

In this expression, the normal-force-curve slope is the tail-alone value, and the term $[(S_t/S)(l_t/\bar{c})]$ is the tail volume coefficient. The quantities α_t and q_t/q, the tail angle of attack, and tail dynamic pressure ratio generally describe the

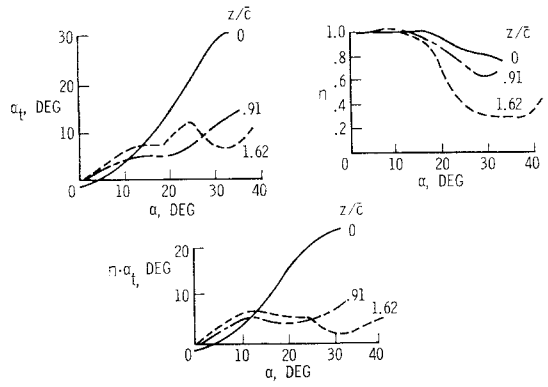

Fig. 5 Effect of tail height.

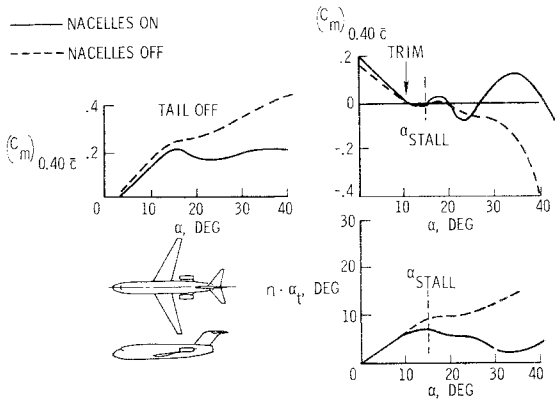

Fig. 6 Effect of aft engine nacelles (basic configuration; $M = 0.21$).

conditions in the flowfield for stability purposes. In this paper, it will be convenient to redefine these quantities such that the normal-force slope $(dC_N/d\alpha)_t$ is the "installed" value on the model, and the tail dynamic pressure ratio q_t/q will be replaced by a factor η that accounts for the angle-of-attack effect on the installed tail normal force. The factor η is called the tail efficiency factor and is obtained by a ratio of the tail-pitch-effectiveness:

$$\eta = C_{m_{it}}/(C_{m_{it}})_{\alpha=0}$$

The tail increment then is written as

$$\Delta C_{m_t} = [(dC_N/d\alpha)_t V_t][\alpha_t \eta]$$

The first bracket is primarily geometry-dependent, and the second bracket is dependent on the variations with angle of attack of the flowfield at the tail. The tail angle of attack may be written as $\alpha_t = \alpha - \epsilon + i_t - i_w$. The tail and wing incidence terms are considered constant, and the variations with angle of attack, then, are attributable to the term ϵ, the downwash angle. The importance of changes in the tail contribution to pitching moment caused by changes in the tail flowfield may be assessed by an examination of tail angle of attack and the tail efficiency factor for the three tail heights presented earlier. Figure 5 shows these data plotted against airplane angle of attack. Below an angle of attack of 10° where η is essentially unity, the increases in stability with tail height noted earlier are in the direction to be explained by the increases in the slope of α_t with increased tail height. The variation in the slope of α_t above wing stall for the solid curve is characteristic of low tails and is caused by the tail emerging from the downwash field behind the wing. An examination of the variation of the tail efficiency factor η with angle of attack shows graphically that, the higher the horizontal tail is placed on the fin, the worse it suffers as the

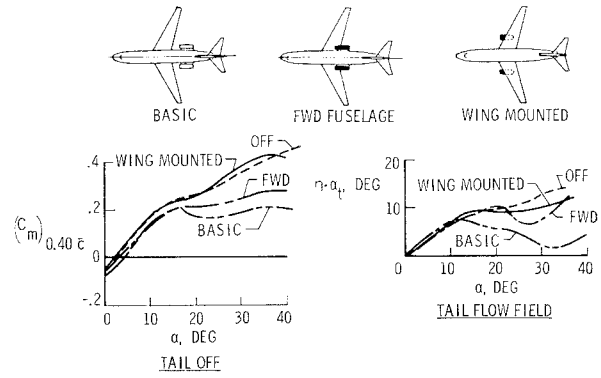

Fig. 7 Effect of nacelle location on tail-off pitching-moment coefficient and tail flowfield.

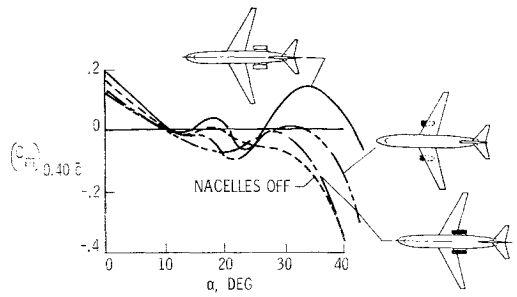

Fig. 8 Effect of nacelle location on pitching moment.

angle of attack increases. Again, it should be emphasized that the tail efficiency factor η reflects only angle-of-attack effects, for example, tail nonlinearities and the changes in q_t/q associated with angle of attack. At an angle of attack of 35°, the relative efficiencies are about 0.70, 0.50, and 0.30 of the low-lift value as the tail goes from $z/\bar{c} = 0$ to 1.62. Where convenient throughout the paper, both the tail efficiency factor η and the tail angle of attack α_t are examined together by combining them into a flowfield parameter $[\eta\alpha_t]$, as shown in the bottom of the figure. For the highest tail increment, the product should be a maximum. The tail contribution to stability $\Delta C_{m_{\alpha,t}}$ is proportional to the slope of the curve $\eta\alpha_t$ times the geometry coefficient. For the highest stability from a given tail, the slope should be highest.

The characteristics of the low tail shown in the bottom plot allow its use to overcome poor stalling patterns of more highly swept wings and provide over-all good stability characteristics past wing stall. The high tail, on the other hand, shows a very poor variation with angle of attack past stall which reflects in the moment curve exhibiting a high-angle trim point.

Effect of Engine Nacelle Location

The influence of the nacelles on the tail moment was shown in Ref. 3. Figure 6 represents the variation of pitching-moment coefficient with angle of attack with nacelles on and off for both tail-on and tail-off conditions. The influence of model angle of attack on the flowfield parameter with nacelles on and off is also presented.

It was pointed out in Ref. 3 that the predominating detrimental influence of the nacelle was a blanketing of the tail by the nacelle wake, since the nacelle has a stabilizing effect with the tail off, as shown in Fig. 6. The variation of the flowfield parameter indicates the effect of the nacelles. The nacelles have an influence on the tail past an angle of attack of about 10°, but this flowfield effect is offset by the favorable tail-off moment out to an angle of attack of about 25°, after which the net nacelle increment is positive to very high angles.

Since the nacelle effect was shown to be powerful, ways were sought early in the program to minimize it. The first attempts at improving the situation dealt with relocating the nacelles on the basic configuration. Figure 7 shows the tail-off pitching-moment curves as well as curves of the flowfield parameter with the nacelles off and for three nacelle locations. Data for these locations were given in Ref. 2 and were compared on a nacelles-on/nacelles-off basis with a tail incidence, $i_t = 0$. The effect of moving the nacelles on the tail-off pitch curve is seen to be destabilizing at high angles of attack as the nacelles are moved forward. However, the effect of the nacelles on the tail flowfield shows a definite improvement over the basic location, especially in the region before $\alpha = 20°$. The net effect of these changes is shown in Fig. 8 in the form of pitching-moment coefficient as a function of angle of attack for the complete model with the nacelles off and in the three locations discussed.

Both alternate locations show improvement in the pitch curve over the basic location. With the nacelles on the wing, the tail could be lowered and thereby eliminate the stability difficulty; however, the performance advantages claimed for the T-tail arrangement are lost in the process.

Other modifications were attempted in the area of the nacelle to isolate the effect of the pylon. The buildup of the pylon-nacelles curve is compared with the nacelles-off curve in Fig. 9. Each nacelle for the pylon-off curves was supported from the fuselage by using two pins (shown as dashed lines in the sketch).

The effect of the pylon in the presence of the nacelle is about equal to that for the nacelle alone in destabilizing the trimmed pitch curves. For the curves obtained with the tail off, the pylons plus the nacelles were more stabilizing over a greater angle-of-attack range than the nacelles alone; however, the pylons interfered with the flowfield at the tail to a greater extent. These curves suggest the possibility of mounting the nacelles on pylons from the upper surface of the wing, although this type of pylon was not examined. The results also suggested that the pylon might be reduced in size (within practical limits) to gain some of the benefits noted here. These experiments were disappointing, however, since the complete-configuration pitching moment recorded no change as a result of reducing the pylon chordwise extent by one-half. Attempts at venting the pylon with a 20% gap also proved futile; therefore, the pylon size reduction required to obtain these benefits is impractical.

Another variation in the design of the pylon is shown in Fig. 10, where the results are compared with the basic pylon data. The pylon was attached at the top of the nacelle and at the top of the fuselage as shown in the sketch. This pylon was intended to combine the nacelle wake with the spanwise flow on the swept-forward pylon and carry it inboard close to the fuselage in the hope that the T-horizontal tail

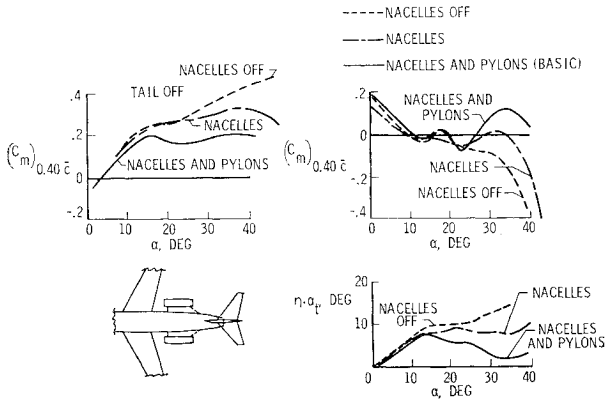

Fig. 9 Effect of pylons on pitching moment.

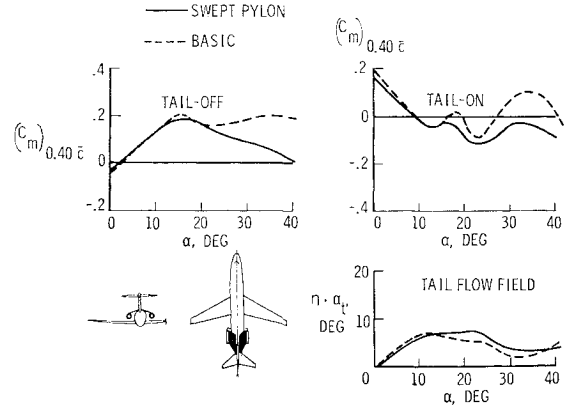

Fig. 10 Effect of pylon modification.

would become more effective. In addition, this pylon results in a substantial amount of the plan area being behind the nacelle as indicated. The results show an improved high-angle variation of the pitch curve. An examination of the details showed that, although the tail effective angle of attack benefited to some extent from the modification, the large effect was an improvement in the tail-off moment curve at high angles of attack, associated with the more rearward location of the pylon area.

In summary, the nacelle effects observed are as follows. Moving the nacelle forward reduces the tail-off stability but increases the tail contribution to the extent that the moment curve is improved. The wing-mounted nacelles reduced the tail-off stability even more and provided a good tail contribution. Pylon effects are as important as the net nacelle effects. Extending the pylon aft improved the pitch curve by providing an improvement in the tail-off configuration and at the same time yielded a small improvement in the tail flowfield.

Effect of Horizontal Surfaces

Another approach investigated was an increase in the size of the horizontal tail or the addition of auxiliary tail surfaces. Figure 11 summarizes some of the configurations that were tested with various horizontal surfaces (see sketches). In addition to the direct area contribution, the effect of increasing the size of the T-tail from 22 to 30% is to move the tips of the tail outboard of the nacelle wake and thereby improve the flowfield parameter. Also shown are data for a low auxiliary surface of the same incremental area. Both additions improve the complete-configuration pitch curve beyond the stall, the large tail for the reasons previously stated and the auxiliary tail by improving the T-tail-off pitch curve. It should be noted that both modifications add wetted area to the basic configuration and should be expected to increase the drag somewhat.

Effect of Fuselage Cross-Sectional Area

The effect of the fuselage cross-sectional size on the pitching-moment curves is presented in Fig. 12. The improvement shown in the complete-model moment curve is attributable to expected improvements in the tail-off curve associated with a large reduction of the nonlinear lift on the fuselage forebody. Of particular interest here is the fact that, despite the large change in fuselage forebody lift, there appears to be only a slight improvement in the flowfield at the tail. Fuselage forebody length has an effect similar to the size effect shown in this figure, that is, increases in the fuselage size tend to destabilize the moment curves at high angle of attack because of the direct contribution to the moment but have only a minor effect on the flowfield in the region of the T-tail.

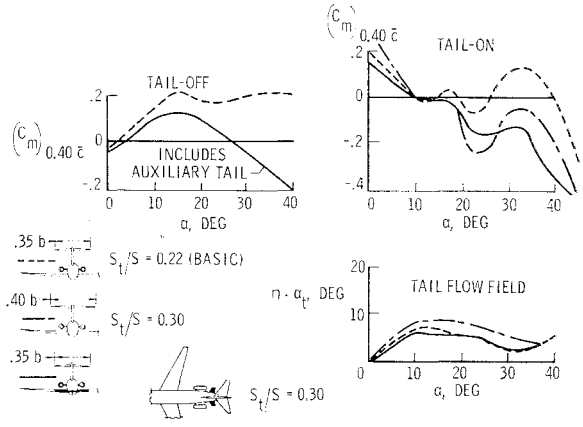

Fig. 11 Effect of horizontal surfaces.

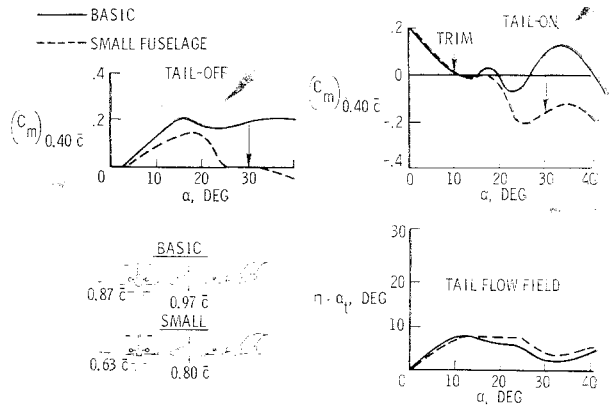

Fig. 12 Effect of fuselage cross-sectional size.

Effect of Nacelles at Other Wing-Sweep Angles

The variation of pitching-moment coefficient with angle of attack for two different wing-sweep angles is presented in Fig. 13. It will be noted that the nondimensional tail height and tail volume are not identical for these two configurations or for either one and the basic configuration that had a sweep angle of 24°. Furthermore, the 12.5° sweep wing had a thickness ratio of only 6% chord with no camber, whereas the 35° sweep wing utilized a NACA 65-412 section. This discrepancy probably accounts for the difference in $(C_L)_{max}$ noted on the figure. The net effect of nacelles is shown by a comparison of the solid and dashed curves for each sweep. The net nacelle moment takes effect at an angle of attack of about 25° at each sweep angle, as well as for the basic data shown earlier. The wing with the higher sweep appears to have less increment due to nacelles by about one-half at an angle of attack of 40°. An interesting comparison was noted in the process of analyzing the data and is presented in Fig. 14. Here the tail angle of attack α_t is shown along with the variation of the tail efficiency factor η with airplane angle of attack. For the tail angle of attack, there appears to be a slight advantage in favor of the 12.5° wing between angles of attack of 15° and 32°. The tail efficiency factor, on the other hand, favors the 35° wing over the same range, probably because of the natural tendency of the more highly swept wing to carry the separated boundary layer spanwise toward the tip. Both of these effects are accounted for in the flowfield parameter $[\eta\alpha_t]$, and for all practical purposes the tail flowfield, and hence, the moment contribution of the horizontal tail is unchanged because of wing sweep.

Effect of Wing Aspect Ratio

Figure 15 shows the variation of pitching-moment coefficient with angle of attack for two wings with different aspect ratios. Since the aspect ratio was changed by clipping the wing tips of the original wing, the nondimensional tail-

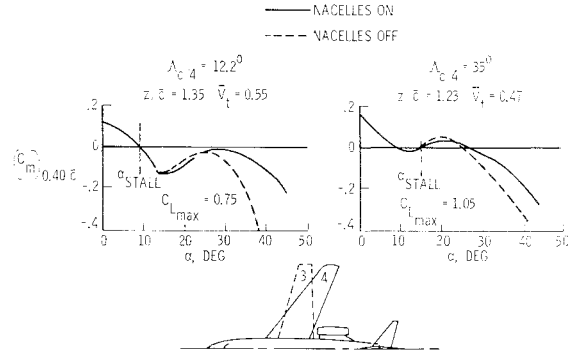

Fig. 13 Effect of nacelles at two wing sweeps.

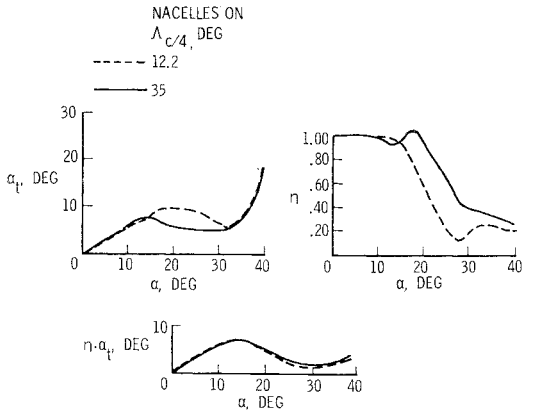

Fig. 14 Influence of sweep on tail flowfield.

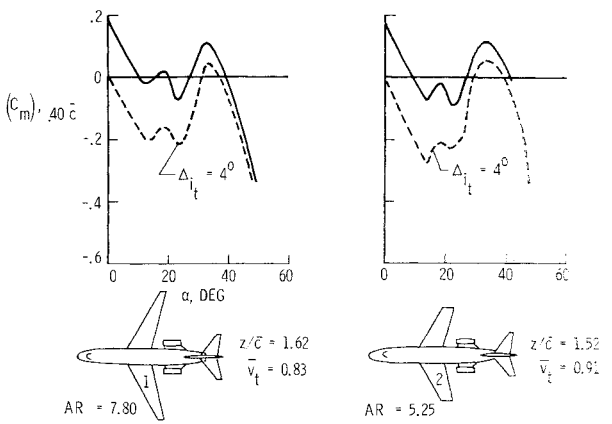

Fig. 15 Effect of wing aspect ratio.

height and tail-volume coefficient changed in the process. The curves show very little effect of aspect ratio in the range of the tests.

Conclusions

Past research on the *T*-tail problem has led to design criteria for the selection of the wing geometry and tail location which appear satisfactory for the prestall stability characteristics. The additional effect of the aft-mounted nacelles is shown to be a nose-up moment at high angles of attack which is caused by interference between the nacelle wake and the horizontal tail.

A number of locations for the nacelles which minimize the nacelle interference at the tail are shown. The importance of the pylon is shown to be about equivalent in magnitude to the net moment of the nacelle itself. Several means are discussed for improving stability after the wing stall, among which are changes in pylon design, changes in tail area, and addition of low auxiliary tail surfaces. The effect of body wake, as determined by changing fuselage size, has only a secondary effect on the flowfield at the tail; the primary effect of increasing fuselage size is the destablizing nonlinear lift forward of the moment reference point. The effect of increasing wing sweep appeared to have diminished the effect of nacelles, although these results are, at present, incomplete. Aspect ratio was shown to have only a minor net effect on the pitching-moment variation with angle of attack.

References

[1] Multhopp, H., "The case for *T*-tails," Aero Digest **70**, 32–35 (May 1955).

[2] Spreemann, K. P., "Design guide for pitch-up evaluation and investigation at high subsonic speeds of possible limitations due to wing-aspect-ratio variations," NASA Langley Research Center, TM X-26 (1959).

[3] Taylor, R. T. and Ray, E. J., "Deep stall aerodynamic characteristics of *T*-tail aircraft," *NASA Conference on Aircraft Operating Problems*, NASA Langley Research Center, SP-83, pp. 113–121 (1965).

[4] White, M. D. and Cooper, G. R., "Simulator studies of the deep stall," *NASA Conference on Aircraft Operating Problems*, NASA Langley Research Center, SP-83, pp. 101–111 (1965).